Designing Bio-Inspired Adhesives for Shear Loading: From Simple Structures to Complex Patterns

*Michael D. Bartlett, Andrew B. Croll, and Alfred J. Crosby**

The gecko has inspired numerous synthetic adhesive structures, yet under shear loading conditions, general design criteria remains underdeveloped. To provide guidance for bio-inspired adhesives under shear, a simple scaling theory is used to investigate the relevant geometric and material parameters. The total compliance of an elastic attachment feature is described over many orders of magnitude in aspect ratio through a single continuous function using the superposition of multiple deformation modes such as bending, shear deformation, and tensile elongation. This allows for force capacity predictions of common geometric control parameters such as thickness, aspect ratio, and contact area. This superposition principal is extended to develop criteria for patterned interfaces under shear loading. Importantly, the adhesive patterns under shear are controlled through the compliance in the direction of loading. These predictions are confirmed experimentally using macroscopic building blocks over an extensive range of aspect ratio and contact area. Over 25 simple and complex patterns with various contact geometries are examined, and the effect of geometry and material properties on the shear adhesion behavior is discussed. Furthermore, all of these various attachment features are described with a single scaling parameter, offering control over orders of magnitude in adhesive force capacity for a variety of applications.

1. Introduction

Many organisms found in nature, such as geckos and insects, possess arrays of fibrillar features on their feet.[1,2] These stiff micro and nanoscale fibrillar features aid in the development of strong adhesive forces while still maintaining a low energy of release, two characteristics required for efficient locomotion. Creating synthetic adhesives that have both strong attachment and easy release is attractive for many potential applications and has driven the design of several synthetic, bio-inspired adhesives.[3–6] Most previous work has focused on normal or peel loading conditions where arguments for contact splitting, *i.e.* breaking an individual contact into numerous smaller contacts, have been developed.[7–10] However, shear loading is employed by organisms during vertical climbing and commonly desired for bio-inspired adhesives, for which design criteria are much less developed.[11] Importantly, the same contact splitting arguments for normal or peel loading cannot be directly applied under shear or other loading geometries as the energy balance at the adhesive interface is fundamentally related to the loading geometry.[12] A robust, general design criteria, especially in the context of shear is required.

The concept of contact splitting states that breaking a single contact into numerous finer subcontacts increases the adhesive pull off force. This is achieved by mechanisms such as softening,[13] an increase in contact line,[10] and crack blunting,[14,15] all of which can be described as a direct consequence of contact splitting. For example, Arzt and co-workers have explained the benefit of an increased contact line through the Johnson-Kendall-Roberts (JKR) model of adhesion,[16] where the pull-off force scales with a geometric length.[10] If a single spherical JKR type contact of radius R_o is divided into an equal area of N smaller contacts of radius R such that $R = R_o/\sqrt{N}$, the pull off force for simultaneous detachment will be increased by a factor of $\sqrt{N}$.[10] The basic Kendall peel model shows that under a 90° peel loading the force capacity will be proportional to the contact width, not the contact area.[17] If a contact is broken into numerous smaller contacts the force capacity will increase as the $\sqrt{N}$.[7] Although these models are attractive, they are restrictive in the choice of geometry and cannot be simply extended to shear loading.[18]

Adhesion under shear loading has been widely studied since the creation of polymeric adhesives.[19,20] Much of the work in this area has focused on long, thin "structural" joints, where the shear stress decays exponentially from the front contact point.[20] This results in the force capacity being independent of the joint's length or contact area, scaling instead as a function of the width.[17] In bio-inspired adhesives, long contact areas are often not made and the assumptions for long, thin "structural" joints are not necessarily appropriate. Previous work in understanding bio-inspired adhesion under shear loading has focused on frictional behavior,[21,22] the coupling between normal and shear adhesive forces,[23–26] and peel arguments to describe

M. D. Bartlett, Dr. A. B. Croll,[+] Prof. A. J. Crosby
Polymer Science and Engineering Department
University of Massachusetts
Amherst, MA 01003, USA
E-mail: crosby@mail.pse.umass.edu
[+] Present address: Department of Physics, North Dakota State University, Fargo, ND 58108, USA

DOI: 10.1002/adfm.201201344

adhesion.[5,27,28] Enhanced friction has been demonstrated with fibrillar adhesives and has been attributed to increased contact area, through softening and side contact of fibrils, but predicting shear capacity has proved difficult.[29]

To understand the broad concepts of bio-inspired adhesion, a unifying relationship is required. Recently, we introduced a scaling argument that was shown to provide a consistent understanding across a large range of length scales and geometries for both natural and synthetic adhesive systems.[30] However, a closer examination is required to determine the implications of these arguments in the general design of both fibrillar and smooth gecko-inspired adhesives. In this paper, we consider a range of adhesive geometries under shear loading, and provide criteria to control the force capacity. We show that superposition can be used to develop simple relationships which describe the deformation behavior over a wide range of sample geometries. These compliance relationships can then be used to predict the adhesive force capacity through our scaling argument described below. We show that in the limit of linear elasticity, superposition can also be used to extend the prediction of force capacity for patterned and complex geometries. Finally, we finish with a discussion on the implications of these results and the scaling relationship in the context of stress and the scaling of adhesives for large and small applications.

2. Design Parameters

2.1. Adhesive Scaling Theory

To develop a general understanding of bio-inspired adhesion, we follow a classical fracture mechanics approach;[31] however, we impose key assumptions appropriate for natural and bio-inspired adhesives to develop a simple scaling theory for adhesive force capacity.[30] A detailed development of this theory has been previously published.[30] In its most simplified form, the fracture mechanics approach relates the energy stored in loading an adhesive interface with the interfacial energy and loss incurred during separation. We consider that an adhesive joint with interfacial area (A) loaded through a force (F) will separate in an unstable manner upon reaching a critical force (F_C). The stored elastic energy ($U_E \propto F^2C$, where C is the system compliance) will be recovered primarily in the form of breaking and forming new surface contacts characterized by the energy U_S or its areal derivative, $\partial U_S/\partial A = -\partial U_E/\partial A = G_C$, where G_C is set by the materials comprising the interface. Within this framework, a scaling relationship for F_C, or the maximum sustainable force, can be written as

$$F_C \sim \sqrt{G_C}\sqrt{\frac{A}{C}} \tag{1}$$

Equation 1 is independent of any geometric or loading details; hence it provides a framework to understand the performance of reversible adhesive systems over a range of geometries and size scales. We note that although many materials are not ideally elastic, Equation 1 is generally applicable to all materials as long as any viscoelastic losses are confined to small-scale regions near the interface, such has been shown for many acrylate, urethane, and siloxane-based polymer networks using a JKR analysis.[31–35]

2.2. Attachment Feature Geometry

To design bio-inspired adhesives which adhere to a wide variety of surfaces the interface should primarily rely upon non-specific van der Waals interactions, as observed in natural gecko setae.[36] This constraint renders G_C an ineffective control parameter. Instead, reversible adhesion is dictated by the geometry of the contact, represented by A and C, which will be the focus of this discussion. For specific geometry and materials, more detailed relationships for A and C can be substituted into Equation 1. Consider a single, bio-inspired attachment feature composed of an adhesive layer with shear modulus μ bound to an adherend with elastic modulus E. The attachment feature has a thickness t and area of contact with the substrate bh, where b and h represent the width and height respectively, as seen in **Figure 1**a.

For a long and thin attachment feature (i.e., a large h and small t) conventionally termed a structural lap shear joint, the crack propagation behavior has been studied by Kendall.[19] In his analysis, the majority of the strain energy is stored in the adherend, and consequently, the strain energy in the adhesive layer is ignored during the fracture analysis and only contributes to the surface energy. In this case, tensile elongation in the adherend defines a force-displacement relationship of $F = \frac{\Delta}{h} Ebt$, where F is the applied force and Δ is the displacement. Accordingly, the compliance $(C = \partial\Delta/\partial F)$ is

$$C_{\text{structural}} = \frac{1}{Eb}\left(\frac{h}{t}\right) \tag{2}$$

For thicker adhesive layers, the deformation will shift from the adherend to the adhesive layer, and the relevant strain energy for crack propagation will be developed in the adhesive layer. A low aspect ratio (t/h) attachment feature will deform through a shear extension with $F = \frac{\Delta}{t}\mu bh$, and the compliance is

$$C_{\text{block}} = \frac{1}{\mu b}\left(\frac{t}{h}\right) \tag{3}$$

For simplicity, we will refer to this as the block geometry.

Attachment features with large aspect ratio (t/h) the applied shear force will deform the material through bending rather than shearing. In the case of negligible shearing, the feature will bend as a cantilever, such that $F = \frac{\Delta}{t^3} 9\mu I$, assuming a Poisson's ratio of 0.5 and I is the beam's second moment of the area $I = \frac{bh^3}{12}$ for a rectangular cross section assumed here. The compliance is

$$C_{\text{post}} = \frac{4}{3\mu b}\left(\frac{t}{h}\right)^3 \tag{4}$$

We will refer to this geometry as the post geometry. We note that a cylindrical post or other cross sections are also used in current generation materials, but this only changes numerical prefactors in compliance and not the scaling.

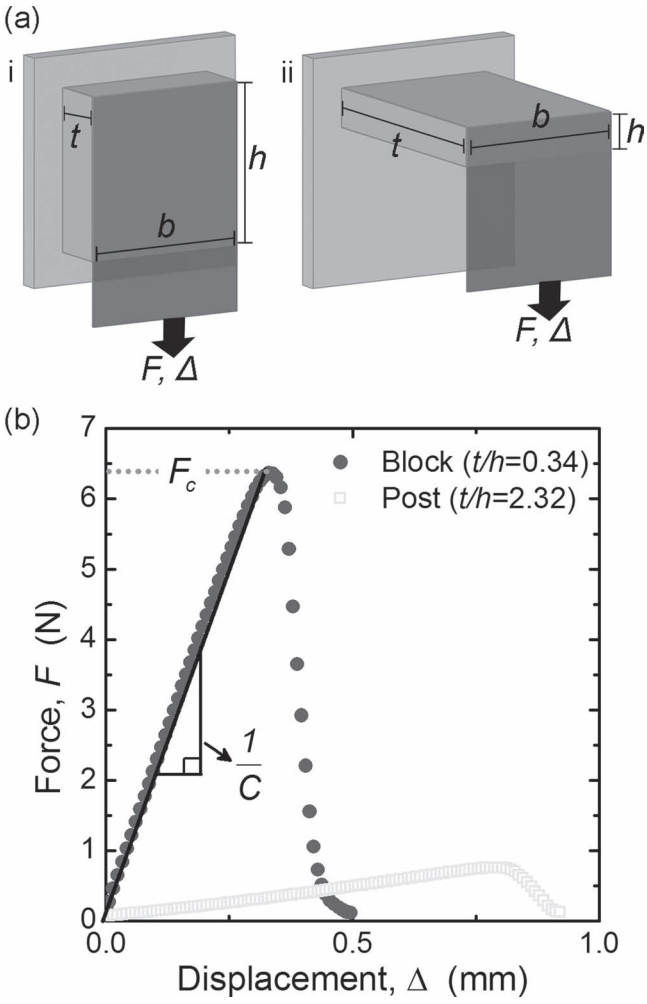

Figure 1. a) Schematics of attachment features consisting of an adhesive layer supported with an adherend with i) low and ii) high aspect ratios (t/h). t is the thickness, h is height, and b is width. After attachment to a glass substrate through a contact area, A (where $A = bh$), a shear force F is applied until adhesive force capacity, F_C, is reached. b) Experimental data showing a typical force versus displacement plot during a shear adhesion experiment for a block and a post. The compliance, C, is the inverse of the slope of the loading curve and upon reaching a critical force capacity, F_C, the interface fails.

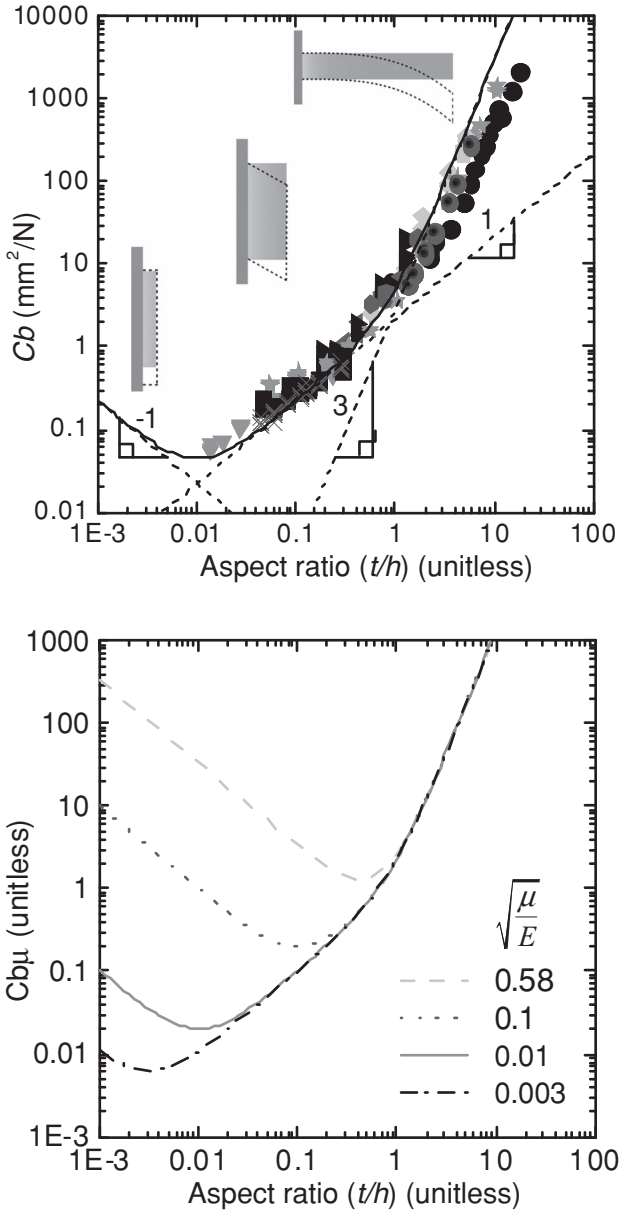

Figure 2. a) A log-log plot of Cb versus aspect ratio (t/h); the various symbol types represent different samples. The dashed lines show a slope of –1, 1, and 3, expected for a structural joint, block, and post, respectively. The solid line is Equation 2, which describes all of the experimental data and is fit with a shear modulus $\mu = 0.45$ MPa ($E = 1.36$ MPa). b) Dimensionless plot of $Cb\mu$ versus aspect ratio for different shear moduli of the adhesive layer, μ, and elastic moduli of the backing layer, E. The upper transition point between the block and post is independent of material properties and occurs at an aspect ratio of $\sqrt{3/4}$, while the lower transition from a structural joint to a block depends on the ratio of the material parameters μ and E.

3. Results and Discussion

3.1. Attachment Feature Compliance

To understand the critical adhesive force as a function of geometric parameters such as thickness and contact area, we create various attachment features with aspect ratios ranging from 0.01 to 17.5, and measure the compliance as a function of aspect ratio. The compliance of a structural lap joint is inversely proportional to aspect ratio (Equation 2), a block geometry is linearly proportional to aspect ratio (Equation 3), and a post scales to the third power (Equation 4). A plot of Cb versus aspect ratio (t/h) is given in **Figure 2**a.

We find good agreement, as seen in Figure 2a, when comparing Equation 2–4 to the experimental data and use these relations to understand the transition regions as the attachment feature goes from one primary deformation mode to another. Near these transition regions, the data deviates from the compliance predictions of Equation 2–4, as the deformation

is no longer due to a single deformation, but instead deforms in a mixed mode.[37] For the case of the lower transition, the feature shifts from tensile elongation to shear deformation. Equating the compliances of the structural joint and the block of the same thickness (see Supporting Information A for different thicknesses), we expect a transition near an aspect ratio of $\sqrt{\mu/E}$. For our system, this occurs at an aspect ratio on the order of $\sqrt{1/10000}$ or 0.01. It is noted that this transition depends on the material system. To describe the upper transition which occurs as shear deformations change to post-like bending, we equate the compliances of the block and the post, which are equal at an aspect ratio of $\sqrt{3/4}$, or approximately 0.87. In contrast to the structural joint to block transition, this transition does not depend on material properties, and is therefore independent of the material system.

To describe the compliance in a unified manner through all of these different transitions, we use the principle of superposition, such that the total deformation of the attachment feature can be treated as a sum of the displacements of the various independent deformation modes. Hence, we serially add these compliances to generate a total compliance

$$C_{\text{Total}} = C_{\text{block}} + C_{\text{post}} + C_{\text{structural}} = \frac{1}{\mu b}\left(\left(\frac{t}{h}\right) + \frac{4}{3}\left(\frac{t^3}{h}\right)\right) + \frac{1}{Eb}\left(\frac{h}{t}\right) \quad (5)$$

It can be seen that Equation 5 describes the structural joint, block and post regions, as well as the transition regions in Figure 2a. Figure 2b shows a dimensionless plot of $Cb\mu$ versus aspect ratio for various $\sqrt{\mu/E}$ ratios. The upper transition point between the block and post is independent of material properties, while the lower transition from a structural joint to a block depends on the $\sqrt{\mu/E}$ ratio.

Equation 5 can be used to describe a wide range of aspect ratios, but for the remainder of the paper we will only be concerned with aspect ratios greater than the lower transition from a structural extension to a sheared block. Thus, for convenience we drop the third extensional term in Equation 5 for investigating the relationship between F_C and attachment feature geometry.

3.2. Adhesive Force Capacity Criteria

The force capacity of an interface depends on the compliance as described in Equation 1. When the compliance of a block or a post is substituted into Equation 1, the critical force scales as $F_C \sim t^{-1/2}$ and $F_C \sim t^{-3/2}$ respectively. To examine this scaling, we keep the contact area constant and vary the thickness. As seen in **Figure 3**a both data sets corresponding to two different interfacial areas follow a $-1/2$ dependence at low thickness and a $-3/2$ dependence at large thickness. At intermediate thickness, a transition from a $-1/2$ dependence to a $-3/2$ dependence is observed as the thickness increases. This is consistent with a block to post transition as observed in the compliance data. We can similarly add the compliance of a block and a post together and substitute the resulting expression into Equation 1 to obtain:

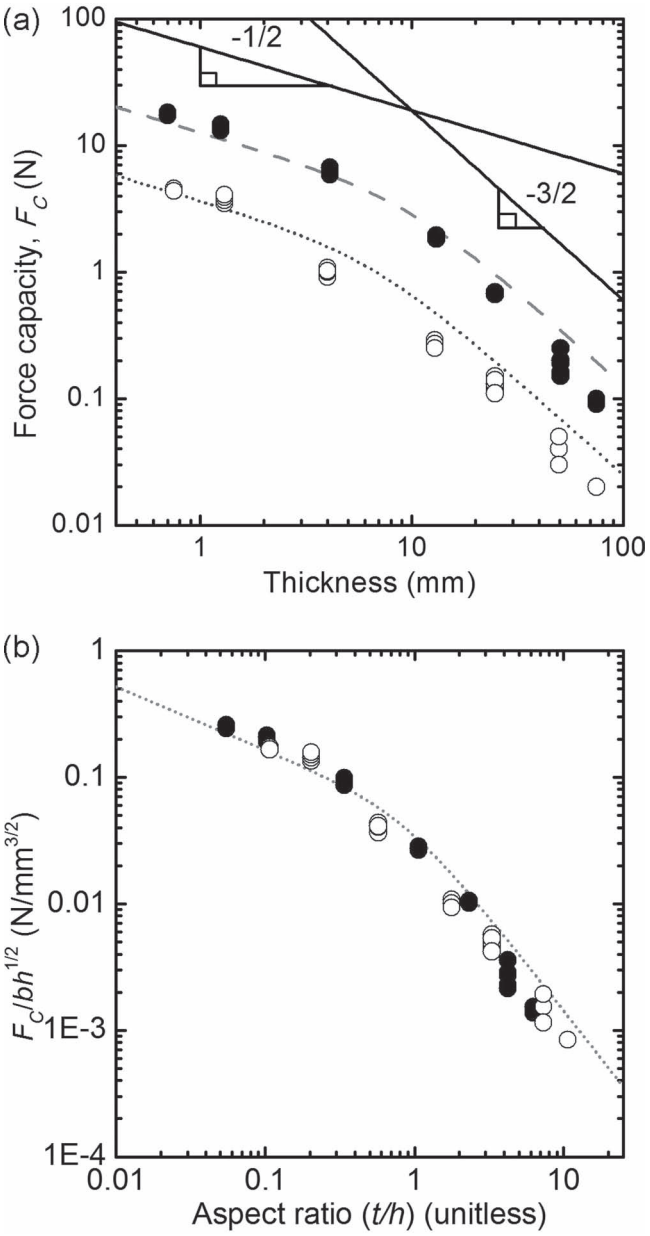

Figure 3. a) Log-log plot of force capacity versus thickness for two different contacting areas, (filled circles: $b = 20$ mm, $h = 12$ mm; open circles: $b = 10$ mm, $h = 7$ mm). The dotted and dashed lines represent the predicted scaling of thickness as seen in Equation 6, where in our experiment $\mu = 0.45$ MPa and $G_C = 3$ N/m, and the solid lines are guides to the eye. b) Log-log plot of normalized force capacity, $F_C/bh^{1/2}$ versus aspect ratio (t/h). The dotted line represents Equation 7, which collapses the data from (a) onto a single line.

$$F_C \sim \sqrt{G_C}\sqrt{\frac{A}{C_{\text{Total}}}} \sim \sqrt{G_C}\sqrt{\frac{\mu b^2 h}{\frac{t}{h} + \frac{4}{3}\left(\frac{t}{h}\right)^3}} \quad (6)$$

This equation describes the data in Figure 3a well. As the two geometries had different contact areas, F_C was always larger for the larger contact area at a constant thickness. To collapse the data onto a single line, the contacting width and height must

be taken into account. Rearranging Equation 6, F_C scales with aspect ratio as

$$\frac{F_C}{bh^{1/2}} \sim \sqrt{G_C}\sqrt{\frac{\mu}{\frac{t}{h}+\frac{4}{3}\left(\frac{t}{h}\right)^3}} \quad (7)$$

By plotting $F_C/bh^{1/2}$ vs. aspect ratio (t/h) the data collapses into a single curve in Figure 3b for a given material. This result shows that although contact area was kept constant the force changed, demonstrating that the adhesive stress capacity was not constant, and that F_C depends on contact area in a more complicated manner.

Equations 6 and 7 both demonstrate, and our experiments confirm, that features with a lower thickness or aspect ratio maximize adhesive force capacities. However, it must be noted that Equations 6 and 7 both assume intimate contact and the experiments were conducted on a smooth glass substrate. If the attachment substrate is rough, then increased compliance normal to the substrate is required to increase A.[13,38] This can be achieved by creating taller features with higher aspect ratios, or decreasing the elastic modulus. In the context of Equation 1, strategies such as tilting fibrillar features and using appropriate backing layers,[5,30,39–43] as demonstrated in the complex anatomy of a gecko's toepad,[11,44] must be used to increase A while maintaining a low compliance in the loading direction to increase the adhesive force capacity.

As demonstrated in the previous section F_C is not necessarily constant for a fixed contact area but depends on the sample thickness. To investigate the F_C dependence on the contact area at constant thickness two samples are used (t = 1.6 mm and t = 50.0 mm) while varying the contact area through changing the contact height. The aspect ratio of the thinner sample is maintained in the block regime ($0.05 < t/h < 0.29$) and the aspect ratio of the thicker sample is in the post regime ($1.3 < t/h < 5.7$). Substituting the compliance of a block into Equation 1, we see that force scales with area, $F_C \sim bh \sim A$; whereas for a post, F_C does not scale with A, but as $F_C \sim bh^2$. In **Figure 4**, we plot F_C/b vs. h for the samples, illustrating that the block and post data scale to the first and second power respectively, as predicted. Interestingly, this demonstrates that normalizing by area to calculate a stress is not always appropriate and depends upon the attachment feature geometry.

3.3. Patterned Shear Adhesion

With a clear description of individual features, we can develop force capacity criteria for arrays of individual features or patterns. An understanding of patterns under normal and peel adhesion has been developed previously.[7,9,10,45] However, the influence of patterns on the adhesive properties under shear loading has not been established.

In the same way that the compliances of an ensemble of springs add together to provide a total compliance, we add the compliance values of individual attachment features to understand how patterns control shear adhesion. If the attachment features are arranged so that they undergo the same displacement, then the compliances add in parallel; if they are arranged so that the total displacement is a summation of individual

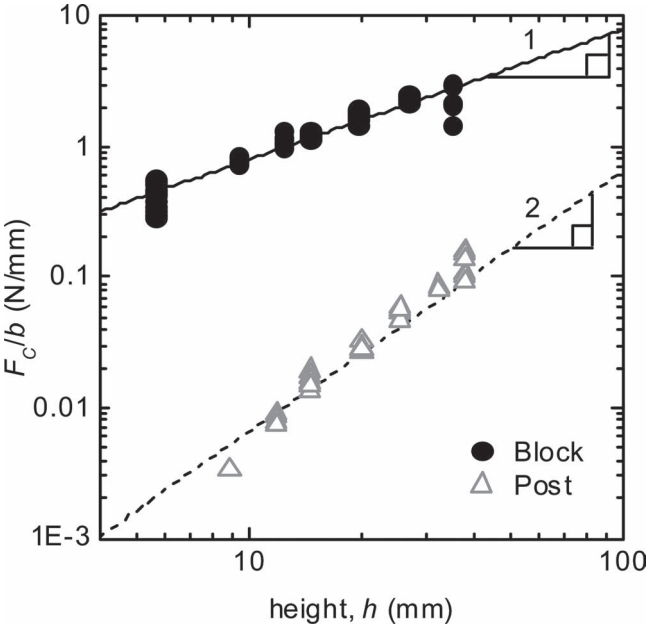

Figure 4. Log-log plot of force capacity over width versus height for two different thicknesses (filled circles: t = 25.3 mm, $0.05 < t/h < 0.29$; open triangles: t = 50 mm, $1.3 < t/h < 5.7$). The black circles are fit to the first power demonstrating block scaling while the open triangles are fit to the second power demonstrating post scaling.

displacements then the compliances add in series. For example, in a hierarchical attachment feature each level will be added together in series, but the individual features in each level are added in parallel. To examine the effects of patterns, we create an array of identical macroscopic PDMS contacts as illustrated in **Figure 5**a. For the simplest case of a single level of non-interacting, identical features attached to a substrate, the compliances add inversely as they are arranged in parallel, giving an ensemble compliance of

$$C = \left(\sum_{j=1}^{N}\frac{1}{C_j}\right)^{-1} = \frac{C_i}{N} \quad (8)$$

Where C_i is the compliance of an individual feature and N is the number features. The total contact area is the sum of the individual attachment feature contact areas, A_i, such that, $A = \sum_{j=1}^{N} A_j = A_i N$. In this case, the total force capacity is proportional to the number of attachment features,

$$F_C \sim \sqrt{\frac{G_C\,(A_i\,N)}{C_i/N}} \sim N\sqrt{\frac{G_C\,A_i}{C_i}} \quad (9)$$

To verify this equation we modulate the number of identical macroscopic PDMS contacts from one to nine. The force vs. displacement plot in Figure 5b shows that as the number of contacts increases the compliance decreases and F_C increases. We verify Equations 8 and 9 in Figure 5c, where it is shown that the compliance scales as $1/N$ and F_C is proportional to the number of contacts. This demonstrates the ability to predict both the compliance, and in turn, F_C of a simply patterned interface by considering the total compliance and contact area.

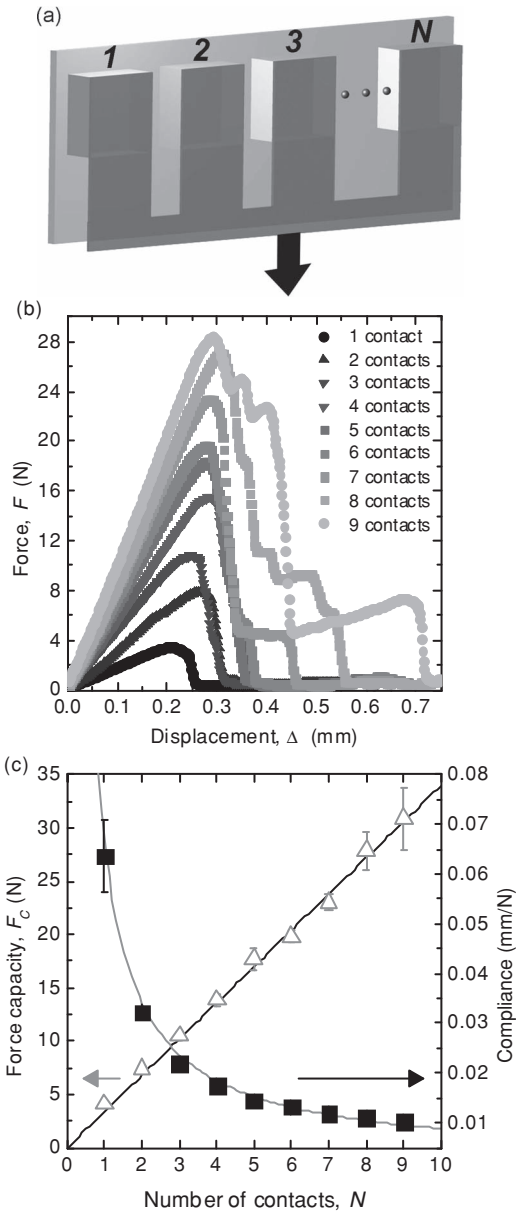

Figure 5. a) Schematic diagram of the identical attachment features loaded in parallel. b) Force versus displacement plot for identical attachment features, ranging from one to nine contacts. c) Left y-axis: force capacity versus the number of attachment features (open triangles) showing the linear relationship predicted by Equation 9. Right y-axis: compliance versus the number of attachment features (filled squares) showing the 1/*N* relationship predicted by Equation 8.

We create more complex hierarchical structures, such as a post between two blocks (**Figure 6**b), multiple posts arranged orthogonal to a single post (Figure 6c), or even setal like features (Figure 6d) consisting on an angled "setal" shaft with multiple terminal contacts (for schematics of the entire set of 20 complex structures tested see Supporting Information B). In these cases, the force capacity will not be proportional to the number of contacts, as each contact is unique, and may add to the compliance in series or in parallel. Instead, the compliance of each individual feature is measured, and then added together to obtain a total compliance and the contact area is only the area which is in contact with the substrate. In this case, features in the same hierarchical level are added in parallel, and different hierarchical levels are added serially. In Figure 6a, a plot of the theoretical force capacity vs. the measured force capacity shows that the data generally lies along a $y = x$ line, showing direct correlation between predictions and the measured values.

3.4. Connecting Blocks, Posts and Patterns

We have shown how the adhesive force capacity depends on geometric parameters such as thickness, aspect ratio, and contact area. We extend this understanding to multiple attachment features to develop criteria for patterned interfaces under shear loading. However, to describe these various attachment features in a single general equation, we revisit Equation 1, which states that the force capacity of a reversibly adhesive interface should scale as the $\sqrt{A/C}$. We use this scaling parameter to describe all of the various geometries, including the blocks, posts, and patterns, by plotting F_C vs. $\sqrt{A/C}$, as seen in **Figure 7**. The $\sqrt{A/C}$ scaling parameter collapses all the various geometries onto a single line, and functions over orders of magnitude in force capacity. As this scaling parameter takes into account the contacting compliance and contact area it allows for various contacting geometries to be described, including patterned and non-patterned interfaces. This is in contrast to scaling adhesive force through the use of stress (force per area), which we have shown to not be appropriate for many contacting geometries. Furthermore, using stress as a metric for scaling adhesion assumes that a small contacting area will behave identically to a large contacting area. This is often not the case because creating contact over increasingly larger contact areas is problematic and load sharing across the adhesive interface is not always constant. Scaling adhesion through the A/C ratio provides a general descriptor for adhesion across many contacting geometries and length scales.

4. Conclusions

We have provided design criteria for bio-inspired adhesives under shear loading, demonstrating a robust, general design relationship between geometry and force capacity. Importantly, we illustrate that a single equation can be used to describe the deformation behavior of an attachment feature over a wide range of aspect ratios. The dependence of maximum force capacity on thickness, aspect ratio, as well as contact area have been predicted and experimentally confirmed. By extending this concept to shear adhesion of patterned geometries, the adhesive force capacity of various designs can be predicted by adding the compliance and contact areas of multiple attachment features. In addition, we have successfully used the $\sqrt{A/C}$ ratio to describe the force capacity of a wide variety of attachment features, emphasizing that maximum force capacity is achieved with features that have sufficient compliance normal to an interface to maximize A while minimizing C, the compliance,

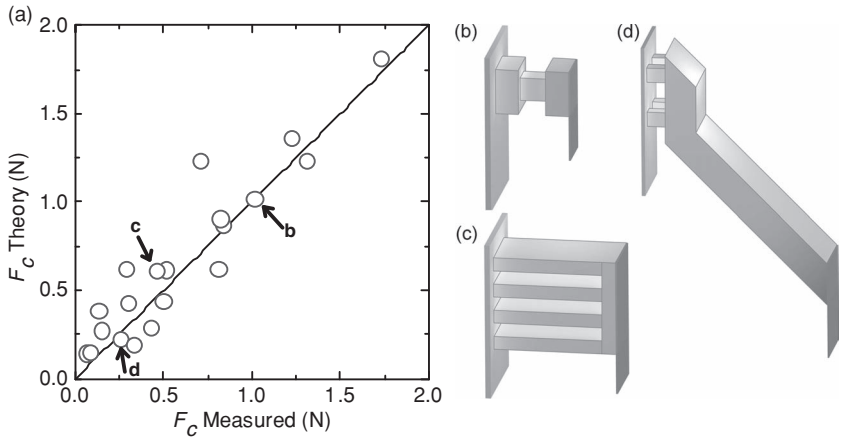

Figure 6. a) Theoretical force capacity versus measured force capacity for a variety of complex patterns, examples of such patterns are depicted by the schematics (–d). The solid line is a $y = x$ line showing agreement between the predicted and measured force capacities.

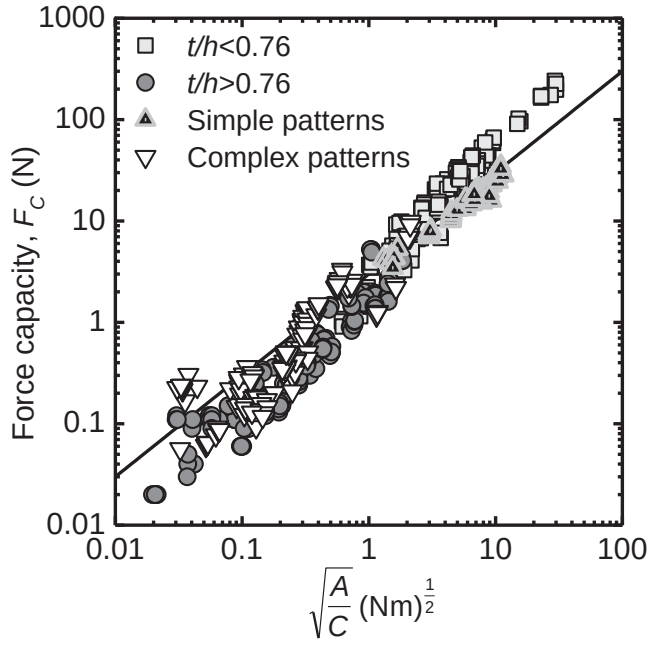

Figure 7. Force capacity (F_C) versus $\sqrt{A/C}$ for all of the tested attachment features, including blocks, posts, and the patterned interfaces. All of the data collapse onto a single line described by the $\sqrt{A/C}$ scaling parameter.

in the direction of loading. The simple guidelines presented in this work lend a clear method for material design and evaluation, offering a fundamental framework in efficiently creating bio-inspired adhesive materials for a variety of applications.

5. Experimental Section

Material Fabrication: Rectangular glass molds were made by fixing glass slides (Dow Corning) with cyanoacrylate adhesive (Loctite Super Glue) to a glass substrate. Before assembly, the glass was cleaned with soap and water, dried with air, cleaned with acetone, and dried again with air. Adhesives were fabricated by filling the molds with oligomeric PDMS and a curing agent (Dow Corning Sylgard 184) 10:1 ratio by mass. A 1K plain weave carbon fiber fabric (Composite Envisions) was used as an adherend and placed on top of the uncured PDMS to allow for incorporation. This was necessary for handling the thin adhesive layers, and also facilitated complete interfacial contact across the PDMS-glass interface. An excess of fabric was used to clamp the adhesive into the testing apparatus. The sample was then cured at 70 °C for 14 h. Simple patterns are then created by mechanically cutting the adhesive material into discrete attachment pads. Complex patterns consisting of individual PDMS building blocks were bonded together using Sil-Poxy silicone adhesive (Smooth-On).

Adhesion Characterization: Shear adhesion experiments were performed with an Instron 5500R on clean glass in lap shear geometry at a displacement rate of 10 mm/min. The adhesives were attached to the glass substrate taking care to ensure that the adhesive made complete contact with the glass. The fabric tether was then attached to the load cell. Displacement and force were measured throughout the experiment as seen in Figure 1.

Supporting Information

Supporting Information is available from the Wiley Online Library or from the author.

Acknowledgements

The authors thank D. King, J. Pham, S. Pendergraph, M. Lis, and C. Davis for thoughtful discussions and suggestions. A.J.C., M.D.B., and A.B.C., acknowledge the US Defense Advanced Research Projects Agency (DARPA) through a sub-contract to Draper Laboratory and the University of Massachusetts research funds for support for this research.

Received: May 17, 2012
Revised: June 25, 2012
Published online: July 23, 2012

[1] K. Autumn, Y. A. Liang, S. T. Hsieh, W. Zesch, W. P. Chan, T. W. Kenny, R. Fearing, R. J. Full, *Nature* **2000**, *405*, 681.
[2] A. P. Russell, *Integr. Comp. Biol.* **2002**, *42*, 1154.
[3] L. F. Boesel, C. Greiner, E. Arzt, A. Del Campo, *Adv. Mater.* **2010**, *22*, 2125.
[4] Q. Liangti, D. Liming, S. Morley, X. Zhenhai, W. Zhong Lin, *Science* **2009**, *322*, 238.
[5] H. E. Jeong, J.-K. Lee, H. N. Kim, S. H. Moon, K. Y. Suh, *Proc. Natl. Acad. Sci. USA* **2009**, *106*, 5639.
[6] H. Lee, B. P. Lee, P. B. Messersmith, *Nature* **2007**, *448*, 338.
[7] E. P. Chan, C. Greiner, E. Arzt, A. J. Crosby, *MRS Bull.* **2007**, *32*, 496.
[8] M. Kamperman, E. Kroner, A. Del Campo, R. McMeeking, E. Arzt, *Adv. Eng. Mater.* **2010**, *12*, 335.
[9] E. P. Chan, E. J. Smith, R. C. Hayward, A. J. Crosby, *Adv. Mater.* **2008**, *20*, 711.
[10] E. Arzt, S. N. Gorb, R. Spolenak, *Proc. Natl. Acad. Sci. USA* **2003**, *100*, 10603.
[11] A. M. Peattie, R. J. Full, *Proc. Natl. Acad. Sci. USA* **2007**, *104*, 18595.
[12] K. Kendall, *J. Phys. D: Appl. Phys.* **1971**, *4*, 1186.
[13] A. Jagota, S. J. Bennison, *Integr. Comp. Biol.* **2002**, *42*, 1140.
[14] H. Gao, H. Yao, *Proc. Natl. Acad. Sci. USA* **2004**, *101*, 7851.

[15] C. Y. Hui, N. J. Glassmaker, T. Tang, A. Jagota, *J. R. Soc. Interface* **2004**, *1*, 35.
[16] K. Johnson, K. Kendall, A. Roberts, *Proc. R. Soc. London Series A* **1971**, *324*, 301.
[17] K. Kendall, *J. Phys. D: Appl. Phys.* **1975**, *8*, 1449.
[18] A. Jagota, C.-Y. Hui, *Mater. Sci. Eng. R* **2011**, *72*, 253.
[19] K. Kendall, *J. Phys. D: Appl. Phys.* **1975**, *8*, 512.
[20] D. H. Kaelble, *J. Rheol.* **1960**, *4*, 45.
[21] M. P. Murphy, B. Aksak, M. Sitti, *J. Adhes. Sci. Technol.* **2007**, *21*, 1281.
[22] C. Majidi, R. Groff, Y. Maeno, B. Schubert, S. Baek, B. Bush, R. Maboudian, N. Gravish, M. Wilkinson, K. Autumn, R. Fearing, *Phys. Rev. Lett.* **2006**, *97*, 18.
[23] K. Autumn, A. Dittmore, D. Santos, M. Spenko, M. R. Cutkosky, *J. Exp. Biol.* **2006**, *209*, 3569.
[24] B. Schubert, J. Lee, C. Majidi, R. S. Fearing, *J. R. Soc. Interface* **2008**, *5*, 845.
[25] C. Majidi, R. E. Groff, R. S. Fearing, *J. Appl. Phys.* **2005**, *98*, 103521.
[26] T. Yamaguchi, N. Gravish, K. Autumn, C. Creton, *J. Phys. Chem. B* **2009**, *113*, 3622.
[27] R. K. Kramer, C. Majidi, R. J. Wood, *Adv. Mater.* **2010**, *22*, 3700.
[28] A. Ghatak, L. Mahadevan, J. Y. Chung, M. K. Chaudhury, V. Shenoy, *Proc. R. Soc. London Series A* **2004**, *460*, 2725.
[29] J. Lee, C. Majidi, B. Schubert, R. S. Fearing, *J. R. Soc. Interface* **2008**, *5*, 835.
[30] M. D. Bartlett, A. B. Croll, D. R. King, B. M. Paret, D. J. Irschick, A. J. Crosby, *Adv. Mater.* **2012**, *24*, 1078.
[31] D. Maugis, M. Barquins, *J. Phys. D: Appl. Phys.* **1978**, *11*, 1989.
[32] A. J. Crosby, K. R. Shull, *J. Polym. Sci. Part B: Polym. Phys.* **1999**, *37*, 3455.
[33] M. Chaudhury, G. M. Whitesides, *Langmuir* **1991**, *7*, 1013.
[34] S. Perutz, E. J. Kramer, J. Baney, C.-Y. Hui, C. Cohen, *J. Polym. Sci. Part B: Polym. Phys.* **1998**, *36*, 2129.
[35] K. R. Shull, *Mater. Sci. Eng. R.* **2002**, *36*, 1.
[36] K. Autumn, M. Sitti, Y. a Liang, A. M. Peattie, W. R. Hansen, S. Sponberg, T. W. Kenny, R. Fearing, J. N. Israelachvili, R. J. Full, *Proc. Natl. Acad. Sci. USA* **2002**, *99*, 12252.
[37] A. N. Gent, A. Meinecke, *Polym. Eng. Sci.* **1970**, *10*, 48.
[38] B. N. J. Persson, *J. Chem. Phys.* **2003**, *118*, 7614.
[39] K. Autumn, C. Majidi, R. E. Groff, a Dittmore, R. Fearing, *J. Exp. Biol.* **2006**, *209*, 3558.
[40] B. Zhao, N. Pesika, H. Zeng, Z. Wei, Y. Chen, K. Autumn, K. Turner, J. Israelachvili, *J. Phys. Chem. B* **2009**, *113*, 3615.
[41] H. E. Jeong, J.-K. Lee, M. K. Kwak, S. H. Moon, K. Y. Suh, *Appl. Phys. Lett.* **2010**, *96*, 043704.
[42] J. Lee, R. S. Fearing, K. Komvopoulos, *Appl. Phys. Lett.* **2008**, *93*, 191910.
[43] J. Yu, S. Chary, S. Das, J. Tamelier, N. S. Pesika, K. L. Turner, J. N. Israelachvili, *Adv. Funct. Mater.* **2011**, *21*, 3010.
[44] A. P. Russell, *Integr. Comp. Biol.* **2002**, *42*, 1154.
[45] M. Varenberg, N. M. Pugno, S. N. Gorb, *Soft Matter* **2010**, *6*, 3269.